Slow Magnetic Relaxation in a Mononuclear Five-Coordinate Cu(II) Complex

Hui-Hui Cui, a Wei Lv, a Wei Tong, b Xue-Tai Chen*a and Zi-Ling Xuec

^aState Key Laboratory of Coordination Chemistry, School of Chemistry and Chemical Engineering, Nanjing University, Nanjing 210023, China

^bAnhui Province Key Laboratory of Condensed Matter Physics at Extreme Conditions, High Magnetic Field Laboratory of the Chinese Academy of Science, Hefei 230031, Anhui, China. ^cDepartment of Chemistry, University of Tennessee, Knoxville, Tennessee 37996, USA

Abstract:

A mononuclear five-coordinate Cu(II) complex [Cu(12-TMC)Cl][B(C₆H₅)₄] (1) (12-TMC = 1,4,7,10-tetramethyl-1, 4,7,10-tetraazacyclododecane) with distorted square pyramidal geometry has been synthesized and characterized by single-crystal X-ray diffraction, direct-current and alternating-current magnetic measurements and electron paramagnetic resonance (EPR) spectroscopy. The complex displays slow magnetic relaxation under an external dc field. The analysis of the field- and temperature-dependence of the relaxation rates suggests that the slow dynamics of the magnetization is dominated by the Raman - like process in the temperature range of 1.8 K to 11 K under an applied dc field of 0.15 T. In addition, the results of magnetic dynamics for the diluted sample with diamagnetic Zn(II) ions confirms the molecular origin of slow magnetic relaxation.

Introduction

Different from the classical magnetic materials, the magnetic bistability of single-molecule magnets (SMMs)¹ purely originates from an isolated molecule leading to the advantage of small size and high storage density. SMMs have aroused great attention in recent years due to their potential applications in high-density information storage, spintronics and quantum information process.² In most cases, the SMM behavior, i.e., slow magnetic relaxation, is often observed in the systems with negative axial zero-field splitting (D) in combination with a high spin ground state (S), providing an energy barrier to spin reversal (U_{eff}) predicted as $U_{eff} = |D|S^2$ for the molecules with integer spin ground state and $U_{eff} = |D|(S^2 - 1/4)$ for those with a half-integer spin ground state.³ When slow magnetic relaxation comes from a single paramagnetic metal center, such compounds are referred to as single-ion magnets (SIMs). As the simplest system of SMMs, SIMs show various dynamic behaviors through properly modifying the structure and coordination environment. The examples of SIMs based on lanthanide complexes are numerous because of the strong spin-orbit coupling and large magnetic anisotropy resulting from crystal field splitting of the total angular momentum (J) ground states.⁴ Most notably, the dysprosium metallocene complex with the cation $[(Cp^{iPr5})Dy(Cp^*)]^+$ $(Cp^{iPr5} = penta$ -iso-propylcyclopentadienyl and $Cp^* = penta$ -iso-propylcyclopenta pentamethylcyclopentadienyl) has been reported with a record energy barrier of 1541 cm⁻¹ and a blocking temperature of 80 K.5 In comparison, the number of transition-metal complexes displaying similar slow magnetic relaxation is much fewer due to their smaller magnetic anisotropy. Up to now, 3d-ion complexes reported to show SIMs behavior include $V(IV)^6$, Cr(I/II/III), $^7Mn(II/III/IV)$, $^8Fe(I/II/III)$, $^9Co(I/II)$, $^{10}Ni(I/II/III)$ and Cu(II) ions,

among which the Co(II)-SIMs dominated owing to its larger spin-orbital coupling. Recently, the discovery of a linear cobalt(II) complex with maximal orbital angular momentum by Long and coworkers sets a new record of the energy barrier of 450 cm⁻¹ for a 3d-SIM. ^{10b}

For the S=1/2 spin systems, there is no energy barrier to spin reversal created by a large magnetic anisotropy, that hinders the observation of the slow magnetic relaxation. Hence, it is less possible for such systems to exhibit this typical SMM behavior. This could partly explain why only few examples of S=1/2 systems including V(IV), 6 Mn(IV), 8 e Fe(III), 9 a Co(II), $^{10i-j}$ Ni(II) $^{11a-b}$, Ni(III) 11d and Cu(II) 12 ions with low spin state have been reported to display slow dynamic relaxation only under the applied magnetic field. The origin for slow magnetic relaxation is still in debate, and possible mechanisms involved are not clear yet in these S=1/2 systems. In the linear two-coordinate Ni(I)-SIM, the orbital momentum was unquenched, which contributes to the strong magnetic anisotropy, responsible for the SMM properties. 11a In the other S=1/2 systems, spin-orbital coupling has been suggested to result in the g-factor anisotropy, which could be related to slow magnetic relaxation. It should be emphasized that only one mononuclear six-coordinate Cu(II) complex was reported to exhibit slow magnetic relaxation with two relaxation channels. 12

Herein, motivated by these results, we report the second example of Cu(II)-based SIM, an mononuclear five-coordinate Cu(II) complex [Cu(12-TMC)Cl][B(C₆H₅)₄] (1) (12-TMC = 1,4,7,10-tetramethyl-1,4,7,10-tetraazacyclododecane), with a distorted square pyramidal geometry, which has been extensively studied by single-crystal X-ray structure analysis, EPR spectroscopy and magnetic measurements. Different from the six-coordinate Cu(II) complex reported by Boča et al., ¹² the dynamic magnetic properties confirmed that this five-coordinate

Cu(II) complex displays slow magnetic relaxation even under a small external dc field with only one relaxation channel. Furthermore, upon dilution of the complex with the isostructural diamagnetic Zn(II) matrix, alternating current susceptibility data reveal that slow magnetic relaxation originates from the low spin Cu(II) ion.

Results and Discussion

Structural Descriptions. The single-crystal X-ray analysis reveals that complex 1 crystallizes in the monoclinic space group P 2₁/c. Complex 1 has a five-coordinate Cu(II) center residing in a distorted square pyramidal geometry, in which the four-coordinated nitrogen atoms of the 12-TMC ligand form the basal plane while one chloride ion is located in the apical position (Figure 1). Four methyl groups of the 12-TMC ligand lie in the same side of the apical chloride atom with respective to the basal N₄ plane. The lengths of the C-N bond are almost equal [1.477(3)-1.488(4) Å]. As depicted in Table 1, the Cu-N bonds in the equatorial positions are in the range of 2.054(2)- 2.081(2) Å. The apical Cu-Cl bond is much longer [2.3471(7) Å]. The Cu(II) center lies above the basal N₄ mean plane by 0.58(2) Å. The bond angles between the two neighboring nitrogen atoms around Cu(II) ion in the basal plane are in the range of 84.51(9)° to 86.35(9)°, indicating a pseudo- $C_{4\nu}$ geometry.²⁰ The N-Cu-N bond angles with the two opposite nitrogen atoms are almost equal [147.84(8)° and 146.76(9)°] and much smaller than 180°. As an index of the distortion degree between trigonal bipyramidal and square pyramidal configurations, the angular structural index parameter τ was used to systematize the geometry of the complex, which is defined as the difference between the two largest angles divided by 60.20 Compared to the values of $\tau = 0$ for a perfectly square pyramid and $\tau = 1$ for a perfectly trigonal bipyramid, the τ value of 0.02 was obtained for complex 1, indicating a nearly square pyramidal geometry. Moreover, the continuous shape measurement analyses (*CShMs*) was calculated by using the SHAPE program²¹ to afford a value of 0.37, preferring to the square pyramid (Table S2). The shortest intermolecular Cu–Cu distance is 6.47(3) Å.

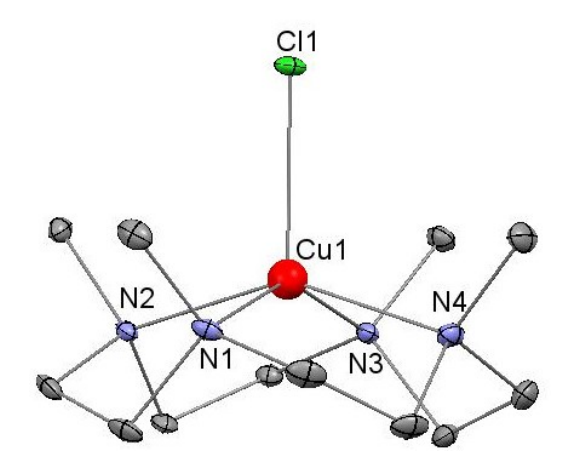


Figure 1. Crystallographic structure of the anion of **1**. Hydrogen atoms have been omitted for clarity. Color codes: Cu, red; N, blue; Cl, green; C, grey.

Table 1. Selected bond lengths (Å) and angles (deg) for complexes 1 and 2.

1		2	
Cu1-N1	2.057(2)	Zn1-N1	2.163(3)
Cu1-N2	2.054(2)	Zn1-N2	2.170(3)
Cu1-N3	2.073(2)	Zn1-N3	2.162(3)
Cu1-N4	2.081(2)	Zn1-N4	2.174(3)
Cu1-Cl1	2.3471(7)	Zn1-Cl1	2.2002(9)
N1-Cu1-N2	85.43(9)	N1- Zn1-N2	82.63(10)
N1-Cu1-N3	147.84(8)	N1- Zn1-N3	137.47(10)
N1-Cu1-N4	86.35(9)	N1- Zn1-N4	81.69(10)
N2-Cu1-N3	85.54(8)	N2- Zn1-N3	82.10(10)
N2-Cu1-N4	146.76(9)	N2- Zn1-N4	136.38(10)
N3-Cu1-N4	84.51(9)	N3- Zn1-N4	82.61(10)
N1-Cu1-Cl1	104.93(6)	N1- Zn1-Cl1	110.78(8)
N2-Cu1-Cl1	107.14(6)	N2- Zn1-Cl1	110.24(8)
N3-Cu1-Cl1	107.23(6)	N3- Zn1-Cl1	111.74(7)
N4-Cu1-Cl1	106.10(7)	N4- Zn1-Cl1	113.37(7)

The structure of the analogous Zn complex $\mathbf{2}$ has also been determined by X-ray crystallography (Table S1). It exhibits a similar crystal structure with space group of P $2_1/c$ as complex $\mathbf{1}$. The molecular structure is shown in Figure S3 and the bond parameters are listed in Table 1. The similar crystal structures of $\mathbf{1}$ and $\mathbf{2}$ permit us to prepare the diluted sample of

1 in isostructural diamagnetic analogue 2 as the matrix, which is useful for the studies of EPR spectroscopy and dynamic magnetic properties (see below).

Static Magnetic Properties. Magnetic susceptibility measurements were performed on the polycrystalline sample of 1. Variable-temperature direct current magnetic susceptibility was measured at an applied dc field of 0.2 T in the temperature range of 1.8–300 K (Figure 2). At room temperature, the $\chi_M T$ product is $0.43 \text{ cm}^3 \text{ mol}^{-1} \text{ K}$, corresponding to the value expected for an S=1/2 ion with g=2.140, which is slightly higher than the theoretical Curie constant of $0.375 \text{ cm}^3 \text{ mol}^{-1} \text{ K}$ with S=1/2 and g=2.0. With the temperature decreases, the $\chi_M T$ value remains almost constant until 16 K, below which it decreases slowly to $0.42 \text{ cm}^3 \text{ mol}^{-1} \text{ K}$ at 1.8 K. The small drop of the $\chi_M T$ value indicates weak intermolecular antiferromagnetic interactions between Cu(II) spins and thus the presence of temperature independent over the entire temperature range. The field dependence of magnetization data for 1 were collected in a range of 1-7 T at 1.8 K, 3.0 K and 5 K, respectively (Figure 2). As the applied dc field increases, the magnetization value increases gradually to $1.07 N_A \mu_B$ at 1.8 K and 7 T, which approximately reaches saturation, supporting an S=1/2 ground spin state.

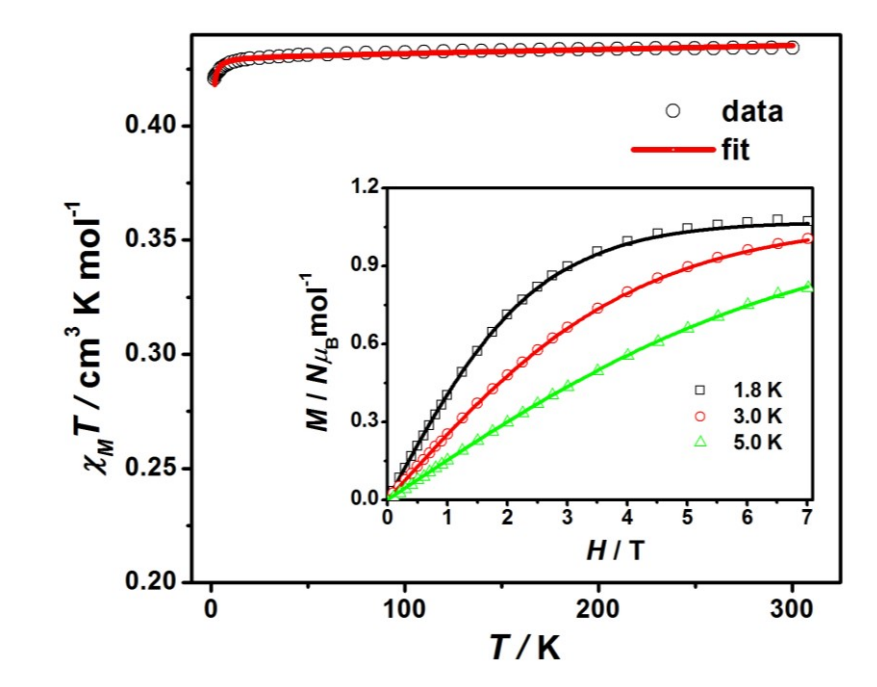


Figure 2. Variable-temperature dc susceptibility data recorded on a polycrystalline sample of **1** at an applied field of 0.2 T. Inset: Field dependence of the magnetization under different temperatures for **1**. Solid lines are fits to the data with the program *PHI*.²²

The experimental variable-temperature magnetic susceptibility and variable-field magnetization data were fitted simultaneously with the PHI^{22} program considering the spin Hamiltonian with three independent anisotropic g parameters, g_x , g_y and g_z . However, the fitting gave the same values for the three g values, $g_x = g_y = g_z = 2.14(1)$, including the correction for the temperature-dependent magnetism χ_{TIP} with $0.16(8) \times 10^{-4}$ cm³ mol⁻¹ and intermolecular interaction at low temperatures zJ with -0.02(4) cm⁻¹.

Electron Paramagnetic Resonance spectroscopy (EPR). For an ideal S = 1/2 spin system, magnetic anisotropy due to zero-field splitting is absent, but structural distortion may result in significant g-factor anisotropy, which can be probed experimentally by EPR spectroscopy.

The X-band EPR spectrum was recorded on the polycrystalline sample of 1 at 4.2 K with a frequency of 9.41 GHz. As shown in Figure 3a, there is one broad feature, which was simulated with an S = 1/2 spin system, yielding the average g value of 2.11, which is in accord with the g_{iso} value determined by the fitting of the magnetic susceptibility.

Figure 3b shows the X-band EPR spectrum of the diluted sample 1' recorded at 4.2 K with a frequency of 9.41 GHz. Three well resolved lines of four were found at low field, which could arise from the interactions of the unpaired electron spins and the copper nuclei, but no clear superhyperfine splitting caused by coupling with the four nitrogen atoms of 12-TMC was observed. The fourth line could be completely overlapped by the much stronger but not resolved signal that appears in the high field region. This observation of the EPR spectrum showing hyperfine and weak signal peaks at lower field has been found for Cu(II) complexes with a square pyramidal geometry.²³ This spectrum was simulated accurately assuming four nitrogen nuclei with identical hyperfine values ${}^{N}A$ and taking into consideration the copper hyperfine coupling ${}^{Cu}A$. The resulting hyperfine coupling constants are ${}^{Cu}A_{||} = 146$ Gauss, ${}^{Cu}A_{||} = 36$ Gauss, ${}^{N}A_{||} = 15$ Gauss and ${}^{N}A_{||} = 15$ Gauss, respectively. Simulation of the spectrum has shown axial symmetry for the Cu(II) complex with $g_{||} = 2.22$ and $g_{\perp} = 2.07$, which demonstrate the significant anisotropy of g tensors. The average g value is 2.12, which is in agreement with the g_{ls0} value of the undiluted complex 1.

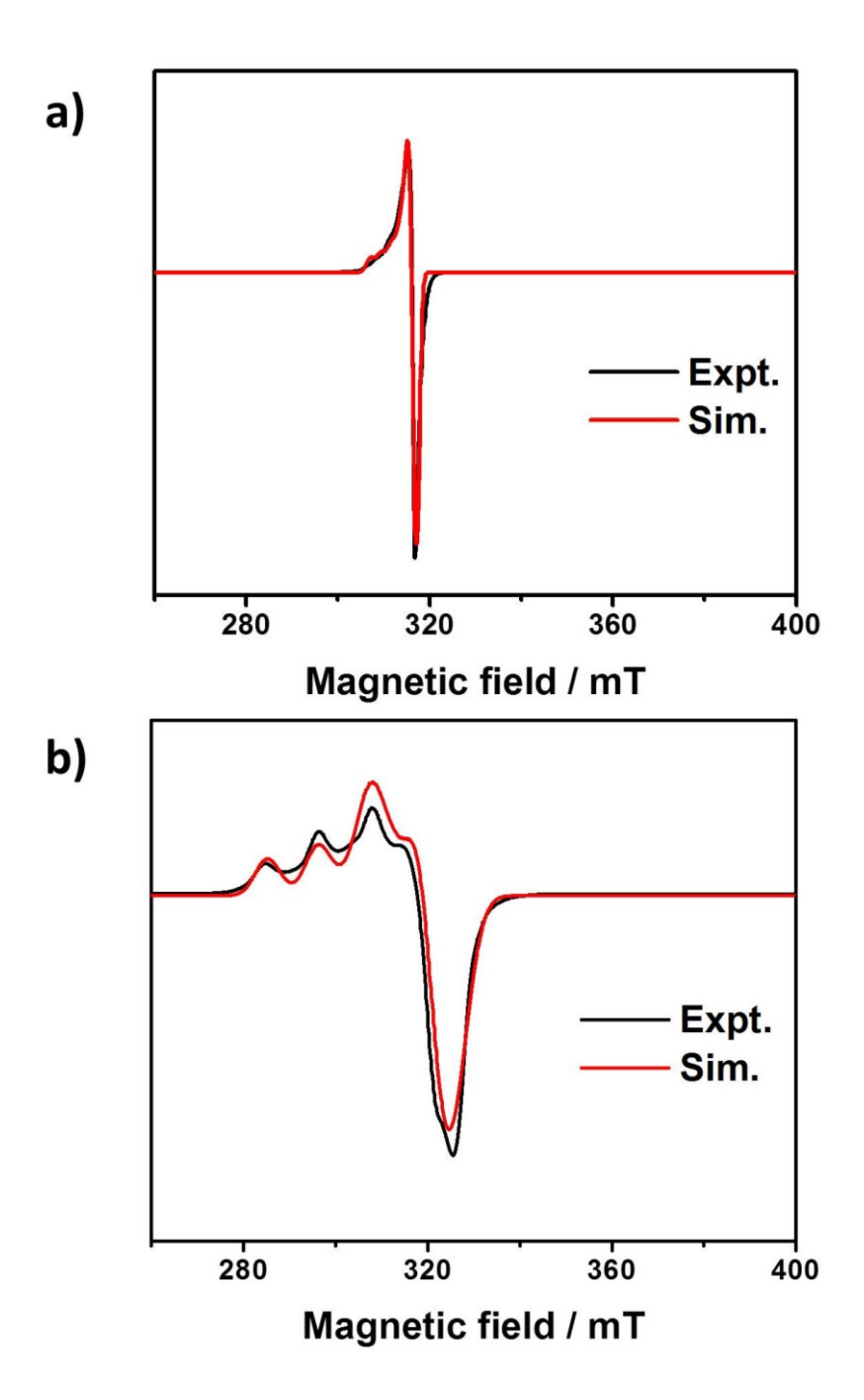


Figure 3. (a) X-band EPR spectrum for **1** at 4.2 K under the frequency of 9.41 GHz. (b) X-band EPR spectrum for **1**' at 4.2 K under the frequency of 9.41 GHz.

Dynamic Magnetic Properties. To probe the magnetic relaxation dynamics, frequency- and temperature-dependent alternative current (ac) susceptibilities of complex 1 were measured under different external dc fields. As shown in Figure S4, this complex exhibits no response

of out-of phase magnetic susceptibility (χ_M ") under zero static magnetic field at 1.8 K. However, a non-zero χ_M " response is observed under an applied external dc field. With the increasing of the external dc field, the χ_M " signal increases in magnitude and the maxima gradually shifts to the lower frequencies, indicating that the magnetic relaxation becomes slower. The χ_M " peak value maximizes at 0.15 T and decreases upon further increasing the dc fields. Therefore, an optimum dc field of 0.15 T was chosen to investigate the further ac magnetic susceptibilities (Figures 4 and S5). Both in-phase (χ_M ") and out-of-phase (χ_M ") susceptibilities show strong frequency-dependence as well as temperature-dependence, indicating the presence of slow magnetic relaxation in 1. Thus, complex 1 behaves as a field-induced SIM.

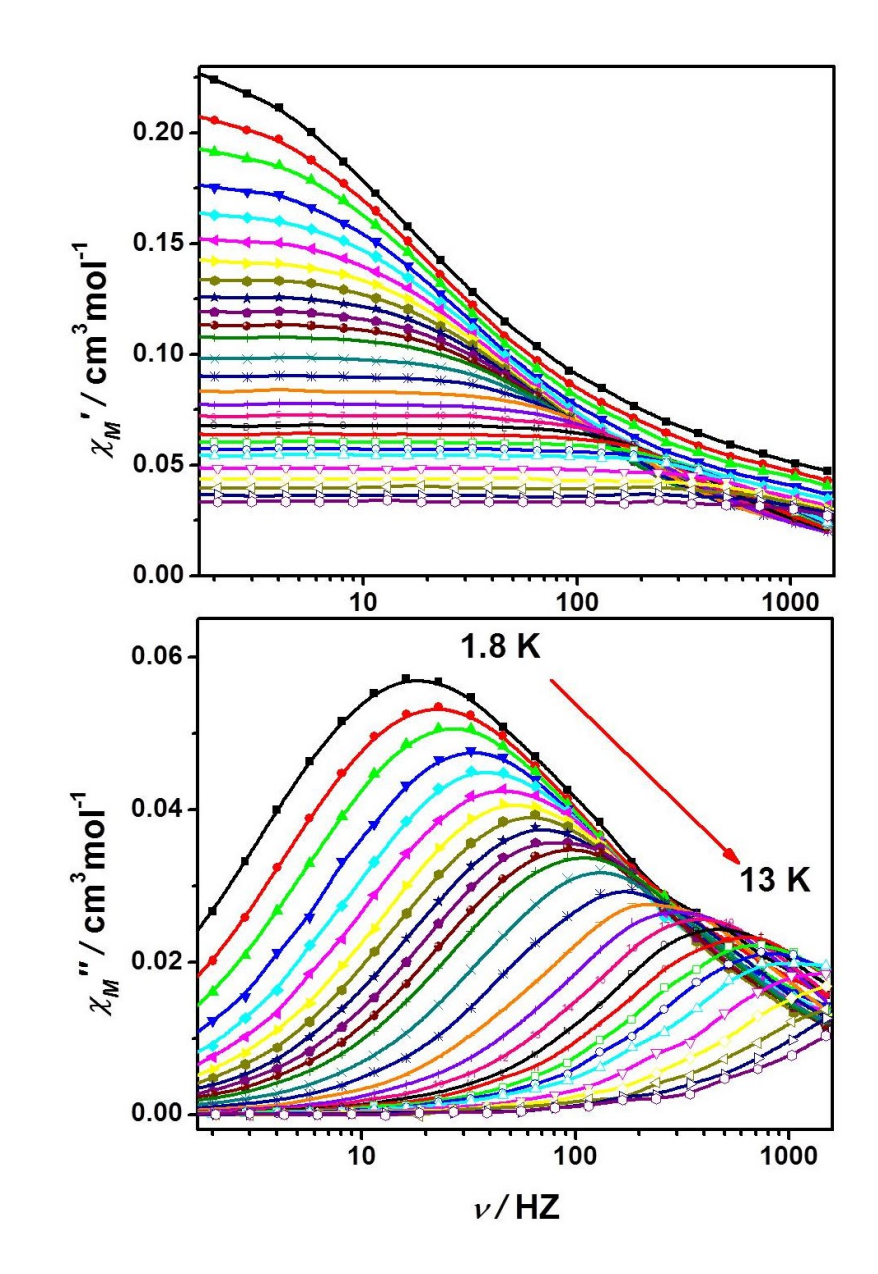


Figure 4. Frequency dependence of the ac susceptibility from 1.8 to 13 K under 0.15 T dc field for **1**. The solid lines are for eye guide.

The frequency values of the maximum in the out-of-phase χ_M " susceptibility from the frequency-dependent data (Figure 4) were used to create the plot of $\ln(\tau)$ versus T^{-1} (Figure 5a), which would provide important information about the magnetic relaxation process by appropriate fitting. Theoretically, there could be several relaxation pathways in magnetic dynamics, including direct, Orbach, Raman and the quantum tunneling of magnetization

(QTM) processes. However, in an S=1/2 system as complex 1, it is obvious that the Orbach process is not possible because of the lack of magnetic/electronic states that can be thermally populated to provide a path for the two-phonon Orbach mechanism. ^{6a,24} Moreover, no reasonable parameters were obtained while considering the QTM process as one of the processes involved. Thus, the plot of $\ln(\tau)$ vs T^{-1} was fitted by a combination of two processes, described by Eq. 1,

$$\tau^{-1} = AT + CT^n \tag{1}$$

where the first term represents direct process and the second term is for Raman or Raman-like process. The successful fit is in accord with the experimental data over the whole temperature range, providing the parameters with A = 52.10(2) s⁻¹ K⁻¹, C = 3.11(5) s⁻¹ K^{-3.59} and n = 3.59(5) (Figure 5a). The value of the exponent n = 3.59 implies a Raman-like process involving both acoustic (lattice) and optical (molecular) vibrations,²⁴ which is unusual compared to the expected value of 9 or higher for the Kramers ion, but has been reported in several recent examples.^{6a-b,8c} Figure 5a shows that the contribution of the Raman-like process is more significant at higher temperatures (from 3 to 9 K) while the direct process is dominated in lower temperature range (from 1.8 to 3 K).

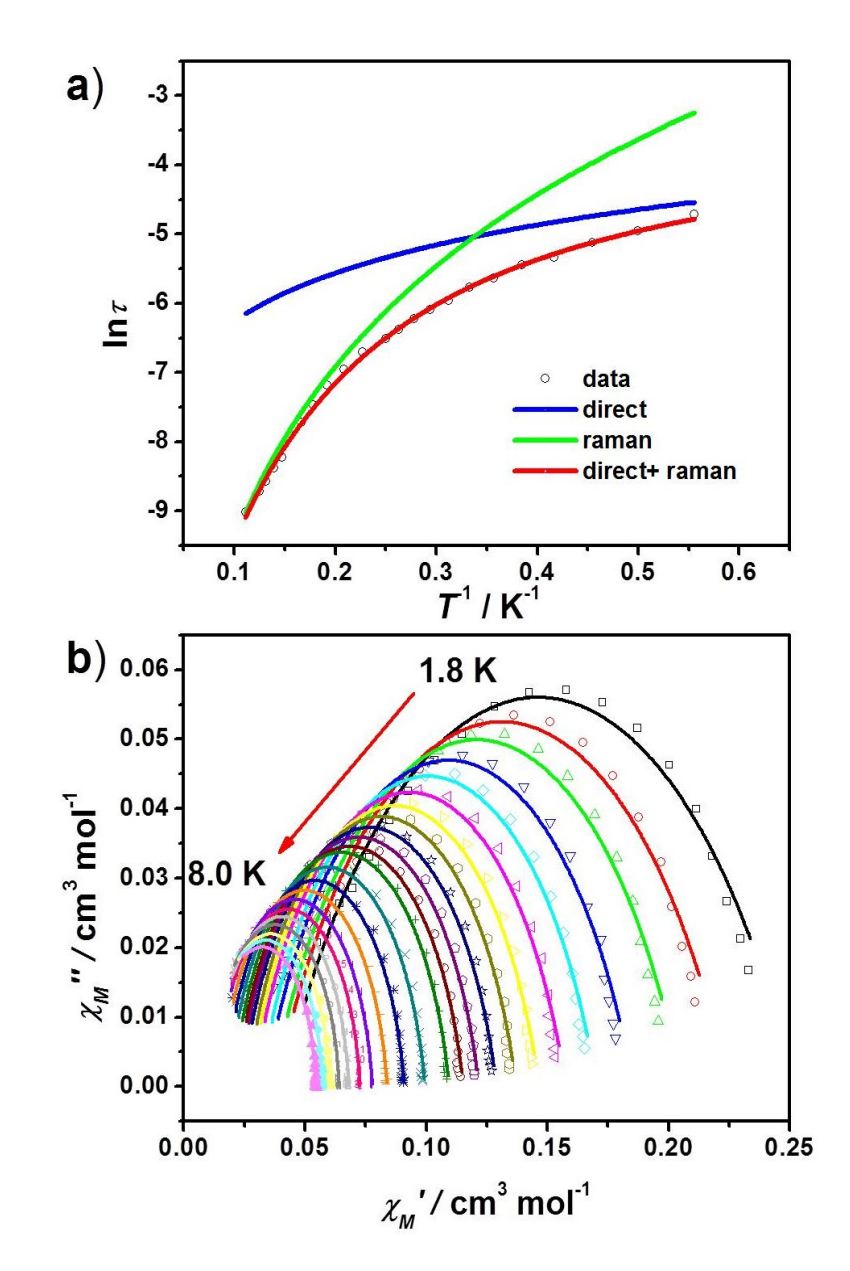


Figure 5. (a) Temperature dependence of the magnetization relaxation rates under a 0.15 T applied dc field for **1**. The red line represents the best fit by using Eq. 1. The other lines represent data fits with the direct (blue) and Raman processes (green). (b) Cole—Cole plots for **1** under 0.15 T dc field. The solid lines are the best fits to the experiments with the generalized Debye model.²⁵

The Cole–Cole plot generated from the ac susceptibility data (Figure 5b) was modeled by the generalized Debye model²⁵ based on Eq. 2 to extract the values and distribution of the

relaxation times:

$$\chi_{ac}(\omega) = \chi_S + \frac{\chi_T - \chi_S}{1 + (i\omega\tau)^{(1-\alpha)}}$$
 (2)

where χ_T and χ_S are the isothermal and the adiabatic susceptibility, respectively; ω is angular frequency; τ is relaxation time; α indicates deviation from a pure Debye model.²⁵ The obtained important fitting parameters are listed in Table S3. The α values are in the ranges of 0.06-0.38 for 1, indicating a narrow distribution of the relaxation times.

In order to gain further insight into the dynamics mechanism in the magnetic relaxation of 1, the magnetically diluted sample [Cu_{0.1}Zn_{0.8}(12-TMC)Cl][B(C₆H₅)₄] (1') was prepared. The diluted complex 1' also displays field-induced slow magnetic relaxation, indicating that slow magnetic dynamics are intrinsic to the central low-spin Cu(II) ion. Similar with 1, an optimum dc field of 0.15 T was chosen to measure the ac magnetic susceptibilities of complex 1' from 1.8 K to 11 K (Figures S6-S8). Compared with the undiluted complex 1, the χ_M " peak values of 1' appeared in the lower frequencies at the same temperatures, indicating slower relaxation in the diluted sample (Figure S7). Moreover, with the temperature increasing, the relaxation time τ extracted from the χ_M " peak values of frequency-dependent data became larger, further indicating the slower relaxation process (Figure 6). The plot of $ln(\tau)$ vs T^{-1} is fitted approximately with Eq. 1, affording coefficient A = 36.98(2) s⁻¹ K⁻¹ for the direct process and coefficients $C = 1.58(1) \text{ s}^{-1} \text{ K}^{-2.66}$ and n = 2.66(1) for the Raman process (Figure S9). As depicted in Figure S9, the direct process is dominated in lower temperature range (from 1.8 to 6.6 K) while the Raman-like process is dominated at higher temperatures (6.6 to 10 K). Obviously the Raman-like process is suppressed and the direct process is more predominant after dilution.

The Cole–Cole plots from the ac magnetic susceptibility data of 1' were also constructed and fitted by the generalized Debye model based on Eq. 2^{25} (Figure S10). The obtained α values are in the ranges of 0.10-0.20, indicating a single relaxation process (Table S4). Qualitatively, the results of magnetic dynamics for the diluted sample ultimately confirms that the slow magnetic relaxation is intrinsic to the individual five-coordinate Cu(II) centre. ²⁶

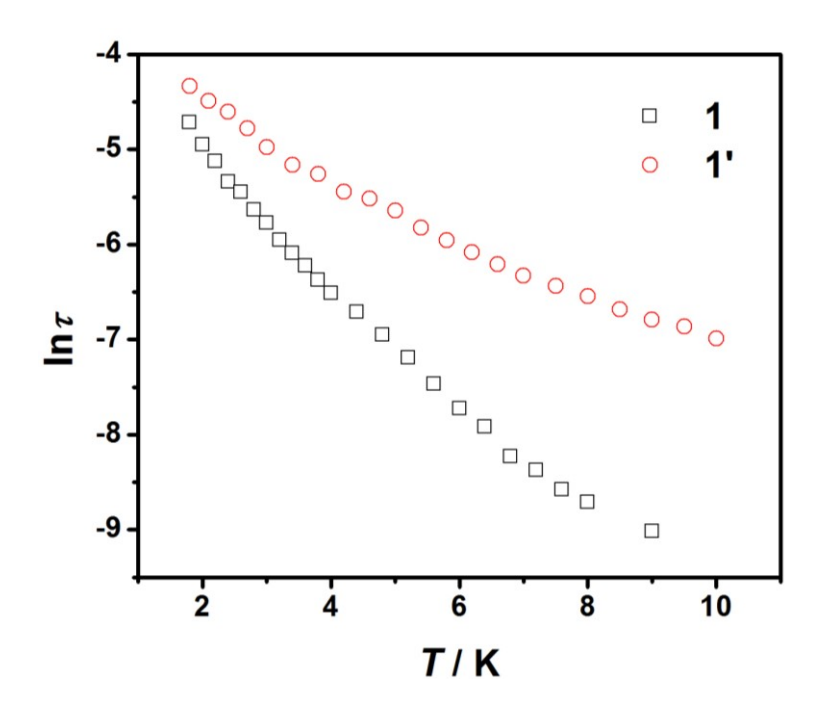


Figure 6. Relaxation time of the magnetization $ln(\tau)$ vs T^1 plot for 1 and 1' under the same dc field of 0.15 T.

As mentioned in the introduction, recent studies reveal that slow magnetic relaxation exists in a few 3d metal-centered mononuclear complexes with low spin S = 1/2 systems. $^{6,8e,9a,10i-j,11a,b,d,12}$ Besides the slow magnetic relaxation in the two-coordinate linear Ni(I)-complex originating to the magnetic anisotropy with unquenched orbital contribution due to its orbital degeneracy, 11a the anisotropic ground doublet due to the spin-orbital

coupling are found in the other S=1/2 systems including V(IV)-,⁶ Mn(IV)-,^{8e} Fe(III)-,^{9a} Co(II)-,^{10i-j} three-coordinate Ni(I)-^{11b} Ni(III)-^{11d} and Cu(II)-¹² SIMs, as revealed experimentally by EPR spectroscopy and/or theoretical calculations. For the five-coordinate Cu(II) complex in this work, the EPR spectra show axial symmetry with two distinct $g_{\parallel} \neq g_{\perp}$ values. Therefore, there still exists a g-factor anisotropy even in the absence of the zero-field splitting. Along this line, the spin-orbit coupling results in the g-tensor anisotropy, representing the magnetic anisotropy in this case. The detailed analysis of the relaxation times reveal the combination of Raman-like and direct mechanisms involved in magnetic dynamic process, which has been suggested for V(IV)-,⁶ Fe(III)-,^{9a} Co(II)-,¹⁰ⁱ Ni(I)-^{11b} and Ni(III)-^{11d} systems. The occurrence of the QTM is in debate, but has been used for the analysis of the relaxation process in Mn(IV)-,^{8e} Co(II)-^{10j} and Cu(II)¹²-SIMs. But the Raman process is found to be dominant in the most cases.

Conclusions

We have reported here a new five-coordinate mononuclear complex $[Cu(12\text{-TMC})Cl][B(C_6H_5)_4]$ (1) that exhibits a distorted square pyramidal geometry. The complex has been studied by X-ray diffraction, EPR spectroscopy as well as magnetic measurements. The experimental results clearly show that complex 1 is a new field-induced SIM with the S = 1/2 ground state. The dynamic magnetic properties show that both direct and Raman-like processes are operative in the spin–lattice relaxation. Importantly, the diluted sample with diamagnetic Zn(II) ions preserves slow magnetic dynamics, further supporting that slow magnetic relaxation originates from the low spin state of the Cu(II) ion. The

foregoing results provide a new example of slow magnetic relaxation for a low spin Cu(II) complex. This study not only enriches the family of Cu^{II}-based SIMs but also extends the scope of SIMs to a broader range of molecules with various spin states. Further efforts will focus on more other metal material displaying slow magnetic relaxation under an unusual spin state.

Experimental Section

General Characterization and Physical Measurements. All manipulations were performed under a nitrogen atmosphere by using standard Schlenk techniques. Ethanol was dried with magnesium using iodine as catalyst and acetonitrile was dried with CaH₂ prior to use. All chemicals were purchased from commercial sources and used as received without further purification, except 1,4,7,10-tetramethyl-1,4,7,10-tetraazacyclododecane (12-TMC), which was synthesized according to the reported procedures.¹⁴ Powder X-ray diffraction (PXRD) patterns were measured for polycrystalline samples on a Bruker D8 ADVANCE X-ray powder diffractometer equipped with a Cu K α X-ray radiation ($\lambda = 1.54056$ Å) over the 20 range of 5° to 50° at room temperature. The phase purity of the samples for magnetic and spectroscopic measurements was verified by the good agreement between the experimental pattern of bulk phase powder X-ray diffraction and simulated one based on the single-crystal structure data (Figures S1-S2, Supporting Information). Elemental analyses (C, H and N) were carried out on an Elementar Vario ELIII elemental analyzer. Inductively coupled plasma-optical emission spectrometry (ICP OES-Optima 5300DV, PerkinElmer Inc., Waltham, MA, USA) was used to confirm the ratio of Zn:Co in the diluted samples.

[Cu(12-TMC)Cl][B(C₆H₅)₄] (1). CuCl₂ (0.5 mmol, 0.067 g) and 12-TMC (1.0 mmol, 0.19 g) were dissolved in 15 mL of ethanol and stirred for 30 min. Na[B(C₆H₅)₄] (1.0 mmol, 0.34 g) was added to the solution and stirred for another 3 h at room temperature to give a cyan precipitate. The precipitate was extracted into 20 mL of acetonitrile and filtered to yield a cyan solution. X-Ray quality crystals were obtained by the slow diffusion of diethyl ether into acetonitrile solution of the product with a yield of 70% based on Co. Anal. Calc. for C₃₆H₄₈BClCuN₄: C, 66.87; H, 7.48; N, 8.66. Found: C, 66.83; H, 7.47; N, 8.68.

[Zn(12-TMC)Cl][B(C₆H₅)₄] (2). 2 was prepared by the same procedure as 1, except using ZnCl₂ (0.5 mmol, 0.069 g) instead of CuCl₂ (0.5 mmol, 0.067 g). The colorless crystals of 2 were obtained in 63% yield based on Zn. Anal. Calcd. for C₃₆H₄₈BClZnN₄: C, 66.68; H, 7.46; N, 8.64. Found: C, 66.65; H, 7.45; N, 8.67.

[Cu_{0.1}Zn_{0.8}(12-TMC)Cl][B(C₆H₅)₄] (1'). The diluted sample 1' was prepared via co-preparation starting with a 1:10 stoichiometry of CuCl₂ and ZnCl₂. CuCl₂ (0.25 mmol, 0.034 g), ZnCl₂ (2.5 mmol, 0.345 g) and 12-TMC (5.5 mmol, 1.045 g) were dissolved in 30 mL of ethanol and stirred for 30 min. Na[B(C₆H₅)₄] (5.5 mmol, 1.87 g) was added to the solution and stirred for another 3 h at room temperature to give a light cyan precipitate. The precipitate was extracted into 60 mL acetonitrile and filtered to yield a cyan solution. The light cyan crystals were obtained from the diffusion of diethyl ether into acetonitrile solution with a yield of 50%. Successful dilution was confirmed by XRD (Figure S2) and ICP data.

X-ray Single-Crystal Structure Determination. Structural characterization was performed with single crystal on a Bruker APEX DUO diffractometer equipped with a CCD area detector using graphite-monochromated Mo Kα radiation (λ = 0.71073 Å). Suitable single

crystal of 1 or 2 was covered with paraffin liquid and placed in a cold stream of N₂ at 155 K. The APEX II program was employed to collect data and determine the unit-cell parameters. The collected diffraction data was integrated and corrected within the SAINT program, ¹⁶ as well as SADABS¹⁷ for absorbance corrections. The molecular structure was solved and refined by using SHELX program (version 2014/7). ¹⁸ All non-hydrogen atoms were refined anisotropically with displacement parameters. And the hydrogen atoms were added at the calculated positions and generated with the riding model. Crystal data and the final refinement parameters of the complexes are listed in Table S1. Additional refinement details were recorded in the corresponding CIF files.

Magnetic Measurements. Magnetic data was collected on a vibrating sample magnetometer (VSM) of Quantum Design MPMS SQUID-VSM system. Measurements were operated on ground microcrystalline powders for the sample sealed in a polycarbonate plastic capsule and restrained in a frozen eicosane matrix to prevent torqueing of crystallites in magnetic field. Direct current (dc) magnetic data were measured at fields up to 7 T in the temperature range of 2–300 K. Besides the diamagnetic corrections applied for the capsule and eicosane, the diamagnetic contribution from the samples were calculated based on Pascal's constants. ¹⁹ Alternating current (ac) susceptibility measurements were carried out at ac frequencies of 1–1500 Hz under different applied dc fields with an oscillating ac field of 0.5 mT.

Electron Paramagnetic Resonance (EPR) Measurement. EPR experiments were

performed on ground microcrystalline powders of the samples on a Bruker EMX-10/12 spectrometer operating at the X-band with continuous helium flow cryostat at 4.2 K under the frequency of 9.41 GHz.

ASSOCIATED CONTENT

* Supporting Information

The Supporting Information is available free of charge on the ACS Publications website at

DOI:

Table for the summary of crystal data and refinement for 1 and 2; Table for the calculations

by SHAPE; Additional figures for magnetic characterization; Table for the fitting data for the

Cole-Cole plot; Additional structural data in CIF format (CIF).

AUTHOR INFORMATION

Corresponding Authors

Email: xtchen@nju.edu.cn

Notes

The authors declare no competing financial interest.

ACKNOWLEDGMENT

We are grateful for the financial support from the Natural Science Grant of China (No.

21471078 to XTC and U1732275 to WT), the National Key Research and Development

Program of China (No. 2016YFA0401802 to WT) and the US National Science Foundation

(CHE-1633870 to ZLX).

21

REFRENCES

- (1) Sessoli, R.; Gatteschi, D.; Caneschi, A.; Novak, M. A. Magnetic bistability in a metal-ion cluster. *Nature* **1993**, *365*, 141–143.
- (2) Mannini, M.; Pineider, F.; Sainctavit, P.; Danieli, C.; Otero, E.; Sciancalepore, C.; Talarico, A. M.; Arrio, M.-A.; Cornia, A.; Gatteschi, D.; Sessoli, R. Magnetic memory of a single-molecule quantum magnet wired to a gold surface. *Nat. Mater.* **2009**, *8*, 194–197.
- (3) Gatteschi, D.; Sessoli, R.; Villain, J. *Molecular nanomagnets*; Oxford University Press: Oxford, **2006**.
- (4) (a) Ishikawa, N.; Sugita, M.; Ishikawa, T.; Koshihara, S.-Y.; Kaizu, Y. Lanthanide double-decker complexes functioning as magnets at the single-molecular level. *J. Am. Chem. Soc.* 2003, *125*, 8694–8695. (b) Woodruff, D. N.; Winpenny, R. E. P.; Layfield, R. A. Lanthanide single-molecule magnets. *Chem. Rev.* 2013, *113*, 5110–5148.
- (5) Guo, F.-S.; Day, B. M.; Chen, Y.-C.; Tong, M.-L.; Mansikkamäki, A.; Layfield, R. A. Magnetic hysteresis up to 80 kelvin in a dysprosium metallocene single-molecule magnet. *Science* **2018**, *362*, 1400-1403.
- (6) (a) Tesi, L.; Lucaccini, E.; Cimatti, I.; Perfetti, M.; Mannini, M.; Atzori, M.; Morra, E.;
 Chiesa, M.; Caneschi, A.; Sorace, L.; Sessoli, R. Quantum coherence in a processable vanadyl complex: new tools for the search of molecular spin qubits. *Chem. Sci.* 2016,
 7, 2074–2083. (b) Atzori, M.; Tesi, L.; Morra, E.; Chiesa, M.; Sorace, L.; Sessoli, R.
 Room-temperature quantum coherence and rabi oscillations in vanadyl phthalocyanine: toward multifunctional molecular spin qubits. *J. Am. Chem. Soc.*

- **2016**, *138*, 2154–2157. (c) Atzori, M.; Morra, E.; Tesi, L.; Albino, A.; Chiesa, M.; Sorace, L.; Sessoli, R. Quantum coherence times enhancement in vanadium(IV)-based potential molecular qubits: the key role of the vanadyl moiety. *J. Am. Chem. Soc.* **2016**, *138*, 11234–11244.
- (a) Samuel, P. P.; Neufeld, R.; Mondal, K. C.; Roesky, H. W.; Herbst-Irmer, R.; Stalke, D.; Demeshko, S.; Meyer, F.; Rojisha, V. C.; De, S.; Parameswaran, P.; Stückl, A. C.; Kaim, W.; Christian, J. H.; Bindra, J. K.; Dalal, N. S. Cr(I)Cl as well as Cr⁺ are stabilised between two cyclic alkyl amino carbenes. *Chem. Sci.* 2015, *6*, 3148-3153.
 (b) Wang, W.-Q.; Li, J.; Yin, L.; Zhao, Y.; Ouyang, Z.-W.; Wang, X.-P.; Wang, Z. -X.; Song, Y.; Power, P. P. Half-sandwich metal carbonyl complexes as precursors to functional materials: from a near-infrared-absorbing dye to a single-molecule magnet. *J. Am. Chem. Soc.* 2017, *139*, 12069–12075. (c) Darawsheh, M.; Barrios, L. A.; Roubeau, O.; Teat, S. J.; Aromí, G. Encapsulation of a Cr^{III} single-ion magnet within an Fe^{II} spin-crossover supramolecular host. *Angew. Chem. Int. Ed.* 2018, *57*, 13509–13513.
- (8) (a) Benniston, A. C.; Melnic, S.; Turta, C.; Arauzo, A. B.; Bartolomé, J.; Bartolomé, E.; Harrington, R. W.; Probert, M. R. Preparation and properties of a calcium(II)-based molecular chain decorated with manganese(II) butterfly-like complexes. *Dalton Trans*.
 2014, 43, 13349–13357. (b) Rajnák, C.; Titiš, J.; Moncol, J.; Mičová, R.; Boča, R. Field-induced slow magnetic relaxation in a mononuclear manganese(II) complex. *Inorg. Chem.* 2019, 58, 991–994. (c) Vallejo, J.; Pascual-Álvarez, A.; Cano, J.; Castro, I.; Julve, M.; Lloret, F.; Krzystek, J.; De Munno, G.; Armentano, D.; Wernsdorfer, W.;

Ruiz-García, R.; Pardo, E. Field-induced hysteresis and quantum tunneling of the magnetization in a mononuclear manganese(III) complex. *Angew. Chem. Int. Ed.* **2013**, *52*, 14075 –14079. (d) Craig, G. A.; Marbey, J. J.; Hill, S.; Roubeau, O.; Parsons, S.; Murrie, M. Field-induced slow relaxation in a monometallic manganese(III) single-molecule magnet. *Inorg. Chem.* **2015**, *54*, 13-15. (e) Ding, M.; Cutsail III, G. E.; Aravena, D.; Amoza, M.; Rouzières, M.; Dechambenoit, P.; Losovyj, Y.; Pink, M.; Ruiz, E.; Clérac, R.; Smith, J. M. A low spin manganese(IV) nitride single molecule magnet. *Chem. Sci.* **2016**, 7, 6132-6140.

(9) (a) Buades, A. B.; Arderiu, V. S.; Maxwell, L.; Amoza, M.; Choquesillo-Lazarte, D.; Aliaga-Alcalde, N.; Viñas, C.; Teixidor, F.; Ruiz, E. Slow-spin relaxation of a low-spin S = 1/2 Fe^{III} carborane complex. Chem. Commun. 2019, 55, 3825-3828. (b)
Zadrozny, J. M.; Xiao, D. J.; Atanasov, M.; Long, G. J.; Grandjean, F.; Neese, F.; Long, J. R. Magnetic blocking in a linear iron(I) complex. Nat. Chem. 2013, 5, 577-581. (c)
Freedman, D. E.; Harman, W. H.; Harris, T. D.; Long, G. J.; Chang, C. J.; Long, J. R. Slow magnetic relaxation in a high-spin iron(II) complex. J. Am. Chem. Soc. 2010, 132, 1224-1225. (d) Feng, X.; Hwang, S. J.; Liu, J. -L.; Chen, Y. -C.; Tong, M. -L.; Nocera, D. G. Slow magnetic relaxation in intermediate spin S = 3/2 mononuclear Fe(III) complexes. J. Am. Chem. Soc. 2017, 139, 16474-16477. (e) Ge, N.; Zhai, Y.-Q.; Deng, Y.-F.; Ding, Y.-S.; Wu, T.; Wang, Z.-X.; Ouyang, Z.; Nojiri, H.; Zheng, Y.-Z. Rationalization of single-molecule magnet behavior in a three-coordinate Fe(III) complex with a high-spin state (S = 5/2). Inorg. Chem. Front. 2018, 5, 2486-2492. (f)
Minato, T.; Aravena, D.; Ruiz, E.; Yamaguchi, K.; Mizuno, N.; Suzuki, K. Effect of

- heteroatoms on field-induced slow magnetic relaxation of mononuclear Fe^{III} (S = 5/2) ions within polyoxometalates. *Inorg. Chem.* **2018**, *57*, 6957–6964.
- (10)(a) Meng, Y.-S.; Mo, Z.; Wang, B.-W.; Zhang, Y.-Q.; Deng, L.; Gao, S. Observation of the single-ion magnet behavior of d⁸ ions on two-coordinate Co(I)–NHC complexes. Chem. Sci. 2015, 6, 7156-7162. (b) Bunting, P. C.; Atanasov, M.; Damgaard-Møller, E.; Perfetti, M.; Crassee, I.; Orlita, M.; Overgaard, J.; van Slageren, J.; Neese, F.; Long, J. R. A linear cobalt(II) complex with maximal orbital angular momentum from a non-Aufbau ground state. Science 2018, 362, 7319(1-9). (c) Deng, Y.-F.; Wang, Z.-X.; Ouyang, Z. W.; Yin, B.; Zheng, Z.-P.; Zheng, Y.-Z. Large easy-plane magnetic anisotropy in a three-coordinate cobalt(II) complex [Li(THF)₄][Co(NPh₂)₃]. Chem. Eur. J. **2016**, 22, 14821–4825. (d) Rechkemmer, Y.; Breitgoff, F. D.; van der Meer, M.; Atanasov, M.; Hakl, M.; Orlita, M.; Neugebauer, P.; Neese, F.; Sarkar, B.; van Slageren, J. A four-coordinate cobalt(II) single-ion magnet with coercivity and a very high energy barrier. *Nat. Commun.* **2016**, 7, 10467(1-8). (e) Jurca, T.; Farghal, A.; Lin, P. H.; Korobkov, I.; Murugesu, M.; Richeson, D. S. Single-molecule magnet behavior with a single metal center enhanced through peripheral ligand modifications. J. Am. Chem. Soc. 2011, 133, 15814–15817. (f) Chen, S.-Y.; Cui, H.-H.; Zhang, Y.-Q.; Wang, Z.-X.; Ouyang, Z. W.; Chen, L.; Chen, X.-T.; Yan, H.; Xue, Z.-L. Magnetic anisotropy and relaxation behavior of six-coordinate tris(pivalato)-Co(II) and -Ni(II) complexes. Dalton Trans. 2018, 47, 10162–10171. (g) Chen, L.; Cui, H.-H.; Stavretis, S. E.; Hunter, S. C.; Zhang, Y.-Q.; Chen, X.-T.; Sun, Y. -C.; Wang, Z.- X.; Song, Y.; Podlesnyak, A. A.; Ouyang, Z.W.; Xue, Z.-L. Slow

Magnetic Relaxations in Cobalt(II) Tetranitrate Complexes. Studies of magnetic anisotropy by inelastic neutron scattering and high-frequency and high-field EPR spectroscopy. *Inorg. Chem.* **2016**, *55*, 12603–12617. (h) Chen, L.; Wang, J.; Wei, J.–M.; Wernsdorfer, W.; Chen, X.–T.; Zhang, Y.–Q.; Song, Y.; Xue, Z.–L. Slow magnetic relaxation in a mononuclear eight-coordinate cobalt(II) complex. *J. Am. Chem. Soc.* **2014**, *136*, 12213–12216. (i) Cui, H. –H.; Wang, J.; Chen, X. –T.; Xue, Z. –L. Slow magnetic relaxation in five-coordinate spin-crossover cobalt(II) complexes. *Chem. Commun.* **2017**, *53*, 9304-9307. (j) Chen, L.; Song, J.; Zhao, W.; Yi, G.; Zhou, Z.; Yuan, A.; Song, Y.; Wang, Z.; Ouyang, Z.–W. A mononuclear five-coordinate Co(II) single molecule magnet with a spin crossover between the *S* = 1/2 and 3/2 states. *Dalton Trans.* **2018**, *47*, 16596–16602.

(11) (a) Poulten, R. C.; Page, M. J.; Algarra, A. G; Le Roy, J. J.; López, I.; Carter, E.; Llobet, A.; Macgregor, S. A.; Mahon, M. F.; Murphy, D. M.; Murugesu, M.; Whittlesey, M. K. Synthesis, electronic structure, and magnetism of [Ni(6-Mes)₂]⁺: a two-coordinate nickel(I) complex stabilized by bulky N-heterocyclic carbenes. *J. Am. Chem. Soc.* 2013, *135*, 13640-13643. (b) Lin, W.; Bodenstein, T.; Mereacre, V.; Fink, K.; Eichhöfer, A. Field-induced slow magnetic relaxation in the Ni(I) complexes [NiCl(PPh₃)₂]·C₄H₈O and [Ni(N(SiMe₃)₂)(PPh₃)₂]. *Inorg. Chem.* 2016, *55*, 2091-2100.
(c) Marriott, K. E. R.; Bhaskaran, L.; Wilson, C.; Medarde, M.; Ochsenbein, S. T.; Hill S.; Murrie, M. Pushing the limits of magnetic anisotropy in trigonal bipyramidal Ni(II). *Chem. Sci.* 2015, *6*, 6823-6828. (d) Bhowmick, I.; Roehl, A. J.; Neilson, J. R.; Rappé, A. K.; Shores, M. P. Slow magnetic relaxation in octahedral low-spin Ni(III)

- complexes. Chem. Sci. 2018, 9, 6564-6571.
- (12) Boča, R.; Rajnák, C.; Titiš, J.; Valigura, D. Field supported slow magnetic relaxation in a mononuclear Cu(II) complex. *Inorg. Chem.* **2017**, *56*, 1478-1482.
- (13) Abragam, A.; Bleaney, B. Electron paramagnetic resonance of transition ions, Dover, New York, **1986**.
- (14) Cho, J.; Sarangi, R.; Kang, H. Y.; Lee, J. Y.; Kubo, M.; Ogura, T.; Solomon, E. I.; Nam, W. Synthesis, structural, and spectroscopic characterization and reactivities of mononuclear cobalt(III)—peroxo complexes. *J. Am. Chem. Soc.* 2010, 132, 16977-16986.
- (15) SMART & SAINT Software Reference Manuals, version 6.45; Bruker Analytical X-ray Systems, Inc.: Madison, WI, **2003**.
- (16) SAINT, Program for Data Extraction and Reduction, Siemens Analytical X-ray Instruments, Madison, WI, **1994–1996**.
- (17) Sheldrick, G. M. SADABS: Software for Empirical Absorption Correction, version2.05; University of Göttingen: Göttingen, Germany, 2002.
- (18) Sheldrick, G. M. SHELXL14: Program for Crystal Structure Refinement; University of Göttingen: Göttingen, Germany, **2014**.
- (19) Bain, G. A.; Berry, J. F. Diamagnetic corrections and Pascal's constants. *J. Chem. Educ.* **2008**, *85*, 532-536.
- (20) Addison, A. W.; Rao, T. N.; Reedijk, J.; van Rijn, J.; Verschoor, G. C. Synthesis, structure, and spectroscopic properties of copper (II) compounds containing nitrogen-sulphur donor ligands; the crystal and molecular structure of

- aqua[1,7-bis(N-methylbenzimidazol-2'-yl)-2,6-dithiaheptane] copper (II) perchlorate. *J. Chem. Soc. Dalton Trans.* **1984**, *3*, 1349-1356.
- (21) (a) Llunell, M.; Casanova, D.; Cirera, J.; Alemany, P.; Alvarez, S. Shape Program,
 Version 2.1, 2013. (b) Alvarez, S.; Alemany, P.; Casanova, D.; Cirera, J.; Llunell, M.;
 Avnir, D. Shape maps and polyhedral interconversion paths in transition metal
 chemistry. Coord. Chem. Rev. 2005, 249, 1693-1708.
- (22) Chilton, N. F.; Anderson, R. P.; Turner, L. D.; Soncini, A.; Murray, K. S. PHI: A Powerful New Program for the Analysis of Anisotropic Monomeric and Exchange-Coupled Polynuclear d- and f-Block Complexes *J. Comput. Chem.* 2013, 34, 1164–1175.
- (23) Umamaheswari, V., Cias, P.; Pöppl, A., Gescheidt, G. Catalytically active
 Cu(II)-pybox complexes: insights by EPR spectroscopy and DFT computations. *Appl Magn Reson* 2014, 45, 667–679.
- (24) Shrivastava, K. N. Theory of spin-lattice relaxation. *Phy. Status Solid B.* **1983**, *117*, 437-458.
- (25) (a) Cole, K. S.; Cole, R. H. Dispersion and absorption in dielectrics I. alternating current characteristics. *J. Chem. Phys.* 1941, *9*, 341–351. (b) Aubin, S. M. J.; Sun, Z. M.; Pardi, L.; Krzystek, J.; Folting, K.; Brunel, L. C.; Rheingold, A. L.; Christou, G.; Hendrickson, D. N. Reduced anionic Mn₁₂ molecules with half-integer ground states as single-molecule magnets. *Inorg. Chem.* 1999, *38*, 5329–5340.
- (26) (a) Schenker, R.; Leuenberger, M. N.; Chaboussant, G.; Loss, D.; Güdel, H. U. Phonon bottleneck effect leads to observation of quantum tunneling of the

magnetization and butterfly hysteresis loops in (Et₄N)₃Fe₂F₉. *Phys. Rev. B.* **2005**, 72, 184403(1-10). (b) Lopez, N.; Prosvirin, A. V.; Zhao, H.; Wernsdorfer, W.; Dunbar, K. R. Heterospin single-molecule magnets based on terbium ions and TCNQF₄ radicals: interplay between single-molecule magnet and phonon bottleneck phenomena investigated by dilution studies. *Chem. Eur. J.* **2009**, *15*, 11390-11400. (c) Meihaus, K. R.; Rinehart, J. D.; Long, J. R. Dilution-induced slow magnetic relaxation and anomalous hysteresis in trigonal prismatic dysprosium(III) and uranium(III) complexes. *Inorg. Chem.* **2011**, *50*, 8484-8489.

(27) Zadrozny, J. M.; Freedman, D. E. Qubit control limited by spin–lattice relaxation in a nuclear spin-free iron(III) complex. *Inorg. Chem.* **2015**, *54*, 12027–12031.